

Non-volatile reconfigurable spin logic device: Parallel operations

Moumita Patra,^{1,*} Alok Shukla,^{1,†} and Santanu K. Maiti^{2,‡}

¹*Department of Physics, Indian Institute of Technology Bombay, Mumbai, Maharashtra-400 076, India*

²*Physics and Applied Mathematics Unit, Indian Statistical Institute,
203 Barrackpore Trunk Road, Kolkata-700 108, India*

(Dated: January 13, 2021)

A new proposal is given for designing a non-volatile, completely spin logic device, that can be reprogrammed for different functional classical logical operations. We use the concept of bias driven spin dependent circular current and current induced magnetic field in a quantum ring under asymmetric ring-to-electrode interface configuration to implement all the Boolean operations. We extend our idea to build two kinds of parallel computing architectures for getting parallelized operations, all at a particular time. For one case, different kinds of parallel operations are performed in a single device, whereas in the other type all the possible inputs of a logic gate are processed in parallel and all the outputs are read simultaneously. The performance and reliability are investigated in terms of power, delay and power-delay-product and finally the system temperature. We find that both the individual and simultaneous logic operations studied here are much superior compared to the operations performed in different conventional logic families like complementary metal oxide semiconductor (CMOS) logic, transistor-transistor logic (TTL), etc. The key advantage is that we can perform several logic operations, as many as we wish, repeating the same or different logic gates using a single setup, which indeed reduces wiring in the circuits and hence consumes much less power. Our analysis can be utilized to design optimized logic circuits at nano-scale level.

I. INTRODUCTION

New generation spin logic gates use up and down spin configurations of electrons as input and output states. The main advantage of a spin logic gate is that it can additionally store output, whereas in the conventional microprocessors, information need to be transferred to memory to prevent it from getting lost, as the electrically processed informations are volatile¹ in nature. Along with it, we can also expect several other key advantages like significantly lower power consumption, fast processing, higher integration densities together with non-volatility, and to name a few. These features are not involved with the conventional logic gates made up with semi-conducting materials²⁻⁵ that belong to CMOS and TTL families. The objectives of this work are to explore the possibilities of designing a non-volatile and reprogrammable spin logic gate with the help of a simple quantum ring, and to extend the idea in devising parallel logic gates.

The underlying physical mechanism of logical operations that we use here relies on the manipulation of bias driven circular current and associated magnetic field in a quantum ring which is attached to external baths. At finite bias, a net circular current appears in the ring conductor satisfying some conditions⁶⁻¹⁴, along with the transport current through the junction which is usually called as the drain current. Appearance of circular current in the conducting loop is directly connected to the effect of quantum interference of electronic waves passing through different arms of the junction. The circular current, on the other hand, induces a magnetic field at and near the center of the ring, and in our analysis we focus on the magnetic field that is developed at the center of the loop. Depending on applied bias and ring-to-electrode interface geometry, the induced magnetic field becomes reasonably large and in some specific situations, it may

even reach to few milliTesla (mT) or even Tesla (T)^{7,10,13}. The strength of the magnetic field is somewhat related with the loop area. Smaller loops yield much stronger magnetic field compared to the bigger ones for a fixed bias window. Existence of finite magnetic field triggers us to think about the logical operations by considering its effect on a (free) spin which is placed at the center of the loop. The induced magnetic field controls the orientation of this local (free) spin^{7,13}. Exploiting this fact, here we design classical Boolean operations where all the inputs and outputs are spin based. Our device is made up of a magnetic quantum ring, with an embedded free

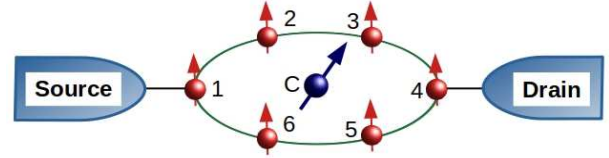


FIG. 1: (Color Online). Basic setup for the construction of logic gates where a magnetic nano ring is coupled to source and drain in such a way that the upper and lower arms acquire equal lengths. Each site of the ring contains a net spin, oriented along Z -direction, as shown by the red arrow. A free magnetic site is embedded at the center of the ring, whose net spin is aligned in an arbitrary direction (blue arrow).

spin at its center, where the ring is directly coupled to two semi-infinite non-magnetic source (S) and drain (D) electrodes (see Fig. 1).

In the magnetic ring, all the lattice sites possess a net spin and among them the orientations (i.e., up or down) of one or two spins, depending on the one-input or two-input logic gates, are considered as the logic inputs. When an electron having a particular spin (up or down) gets incident from the source end, it interacts with the magnetic sites of the ring, which is known as spin-spin

exchange interaction. Because of this, spin channels are separated, and we can get finite spin dependent junction current as well as circular current in the loop. That circular current induces a magnetic field which is utilized to adjust the orientation of the free spin. For the symmetrically connected ring i.e., when the status of the upper and lower arms are identical, circular current vanishes and as a consequence so does magnetic field. Under this situation the alignment of the local spin (not along the Z direction) remains unchanged which we refer as 0 output, while for the case of finite magnetic field, the spin is oriented along $+Z$ which is denoted as output 1. As the output conditions are purely spin-dependent, information can also be stored without giving any extra effort which makes the output a non-volatile one. This is another important advantage over the charged based ones. In this communication, we successfully establish five logical operations (OR, NOT, XOR, XNOR, NAND), employing the above mentioned symmetry condition, and the key feature is that all these logical operations are performed by reprogramming a single setup.

Designing of logic gates where everything is spin based is of great impact, and the efficiency will be enhanced significantly if we can achieve the parallel operations as well. Though some efforts have been made to fabricate nanoscale logic gates, very less amount of works is available so far where parallel operations are explored¹⁵⁻²¹, and thus further probing with a comprehensive discussion is undoubtedly required to have suitable functional operations. This is the primary motivation behind our work. Here, we propose a general concept and specific implementation of individual and parallelized logic devices in two-terminal systems where all parts are spin based. Two kinds of parallel operations are given. In one case, the logical operations are performed in one setup. While, for the other case all the input conditions are implemented at a particular time and all the possible outputs are read simultaneously. Till now a single work is available, to the best of our concern, where Fresch *et al.* have ‘experimentally’ demonstrated how to achieve logic operations where all the inputs are processed in parallel and the outputs are read at the same time¹⁶. In our work, we extended the idea to design the same with non-volatile, spin-based programmability. To fulfill it, we take a logic gate (say, OR gate) as a unit, and add them in parallel where all the input spins align according to four input conditions i.e., (0,0), (0,1), (1,0), and (1,1) and all the corresponding outputs are read at a time. For the entire analysis, we define the input 0 by up spin, while the input condition 1 is mentioned by the down spin one. To have the input conditions 0 and 1, we need to align the spins in the magnetic ring selectively, and several prescriptions are available to control single electron spin. For instance, using radio frequency pulses the spin can be manipulated²²⁻²⁴, though in this case relatively larger time scale is required to operate the spin. On the other hand, the manipulation can be made much faster such as in the picosecond or femtosecond time scale with the help of optical pulses²⁵⁻²⁷. In another pioneering work Press *et al.* have shown that the selective tuning of elec-

tron spin is possible within the spin’s coherence time by means of ultrafast laser pulses²⁸. With the availability of these various sophisticated prescriptions, we strongly believe that the alignment of selective spins in our magnetic quantum ring can be adjusted to implement the desired logical operations.

Here it is relevant to note that the concept of bias driven circular current in a conducting loop in designing individual logic gates has already been reported in a very recent work¹². A cyclic molecule is clamped between two contact electrodes to form a nanojunction where the input signals are given with the help of two external gate electrodes. Only the individual logic operations are explored, without providing any simultaneous logic operations, and all the logic functions are completely charge based. Moreover the concept of ‘spin dependent bias driven circular current’ was not clear during the proposition of logic functions given in Ref.¹². Determination of spin dependent circular current involves the proper definition of spin current components in individual bonds connecting the neighboring lattice sites. First it came into light with a detailed description in Ref.¹⁴, and in the present work we essentially use this concept of spin dependent bias driven circular current to implement individual as well as simultaneous logic operations. This is completely new and has not been attempted so far in literature. Another new concept is that, contrary to the earlier recent proposal of designing parallel logic gates²⁰ where at most two logic functions can be obtained simultaneously at the two outgoing terminals, here we can perform a large number of logic operations, as many as we wish, repeating the identical or dissimilar logic gates, considering a single setup. The limitation of two logical operations in the earlier proposition was mainly due to the fact that the output response is measured in terms of transport current, but this issues is completely eliminated in our present case where we measure the output signal by bias driven spin dependent circular current. Because of this fact multiple operations are performed, all at a time, and the wiring in the circuits largely decreases which eventually reduces power consumption significantly. In Ref.²⁰, the spin-dependent scattering is obtained by means of spin-orbit (SO) coupling. Since this coupling is usually too weak, it is quite hard to produce a considerable separation between the up and down spin channels, and this is the primary requirement to have better spin dependent transport phenomena. This issue can be eliminated by considering a magnetic system, like what is taken in our present work, where spin dependent scattering is too large as the spin-spin exchange coupling is usually of the order of eV²⁹. We believe that the concept of using bias driven spin dependent circular current in a magnetic quantum loop will be the most suitable prescription for designing efficient logic operations.

Along with the designing mechanisms of different logic gates, we put emphasis on the efficiency of such gates under different input conditions. Both the reliability and performance of logic devices are tested in terms of power, delay and power-delay-product (PDP), and finally the system temperature. The PDP, the product of power

dissipation and the delay, is the fundamental quantity that measures the efficiency of a device, and it is the goal of the optimized design to obtain its lowest possible value. From our detailed analysis we find that, both the individual and simultaneous logic operations are much superior compared to the traditional TTL and CMOS logic families. All the above mentioned quantities associated with the device performance viz, power, delay and PDP become extremely small for our systems, and, the key reason of getting smaller values is that here all the logic operations are performed based on ‘spin states’, circumventing the use of ‘charges’ for ON/OFF states as considered in conventional cases. The logical operations are also much less sensitive to the system temperature, which is another key aspect of our propositions.

The rest of the work is arranged as follows. In Sec. II we present the basic magnetic ring setup which is being utilized to have different logic functions and the Hamiltonian of the conducting junction. A brief theoretical prescription is also given in this section. All the essential results are thoroughly presented and analyzed in Sec. III which include both single and the simultaneous logic operations. At the end of results and discussion, we provide a brief outline of designing magnetic nanorings, for the sake of completeness of our analysis. Finally in Sec. IV we summarize our essential findings.

II. QUANTUM SYSTEM AND THEORETICAL PRESCRIPTION

Let us start with the basic setup, schematically illustrated in Fig. 1, where a magnetic nano ring is directly coupled to non-magnetic electrodes S and D. The total Hamiltonian of this nanojunction can be written as a sum

$$H = H_C + H_S + H_D + H_T \quad (1)$$

where H_C , H_S , H_D and H_T represent the sub-Hamiltonians for the channel (C) (viz, the ring conductor), source (S), drain (D), and the tunnel coupling between the ring and the electrodes, respectively. To express these Hamiltonians we use a tight-binding (TB) prescription within a nearest-neighbor hopping (NNH) approximation, which always gives a simple level of description, particularly at nano-scale level. The forms of the sub-Hamiltonians look like

$$H_C = \sum_n c_n^\dagger (\epsilon_n - \mathbf{h}_n \cdot \boldsymbol{\sigma}) c_n + \sum_n (c_{n+1}^\dagger t c_n + h.c.) \quad (2)$$

$$H_M = \sum_n c_n^\dagger \epsilon_0 c_n + \sum_n (c_{n+1}^\dagger t_0 c_n + c_n^\dagger t_0 c_{n+1}) \quad (3)$$

where $M = S, D$. The meaning of different terms are as follows. $\epsilon_0 = \text{diag}(\epsilon_0, \epsilon_0)$ and $t_0 = \text{diag}(t_0, t_0)$, where ϵ_0 and t_0 represent the on-site energy and NNH integrals in the S and D electrodes. $\epsilon_n = \text{diag}(\epsilon_{n\uparrow}, \epsilon_{n\downarrow})$ and $t = \text{diag}(t, t)$, where t is the NNH strength, and $\epsilon_{n\sigma}$ represents the site energy of an electron in the ring in absence

of any magnetic interaction at site n with spin σ ($=\uparrow, \downarrow$). c_n contains the usual fermionic operators $c_{n\sigma}$. The most important term of the above system Hamiltonian is $\vec{h}_n \cdot \boldsymbol{\sigma}$ which is responsible for the spin dependent scattering. $\boldsymbol{\sigma}$ is the vector containing Pauli spin matrices (assuming σ_z as diagonal), and h_n ($=|\vec{h}_n|$) represents the spin-flip parameter. The orientation of \vec{h}_n can in general be described by the usual spherical polar co-ordinates θ_n and φ_n . The strength of h_n is usually very large compared to all other spin-dependent scattering factors, which thus yields a large separation between the up and down spin channels²⁹. This is one of the important motivations behind the consideration of a magnetic ring instead of a SO coupled one, like previous contemporary works. For comprehensive analysis of this of kind spin dependent scattering, see Refs.^{29,30}. Finally, the Hamiltonian H_T that represents the coupling between the ring and contact electrodes is given by

$$H_T = (c_p^\dagger t_{S(D)} c_q + h.c.) \quad (4)$$

where $t_{S(D)} = \text{diag}(t_{S(D)}, t_{S(D)})$. t_S and t_D denote the coupling strengths of the ring with S and D, respectively. p and q denotes the lattice points (those are variable) where S and D are attached to the ring.

This is all about the system Hamiltonian. Using this TB Hamiltonian (Eq. 1) we need to find the required quantities to get the logical operations. The key quantities include (i) bias driven circular current and (ii) induced magnetic field due to this current. We evaluate the first one by determining bond current densities using the wave-guide (WG) theory within the TB framework. In this methodology, a set of coupled equations involving wave amplitudes at different lattice sites of the ring along with the end sites of the electrodes with which the ring is directly coupled are solved. The equations are governed from the Schrödinger equation $H|\phi\rangle = E|\phi\rangle$, where $|\phi\rangle = \sum_i C_{i\sigma} c_{i\sigma}^\dagger |0\rangle$. $C_{i\sigma}$'s are the wave amplitudes. The detailed description of the equations is available in Appendix. A, where the set of coupled equations are written based on the mathematical prescription given in our recent work¹⁴. Here it is relevant to note that, the generalized wave-guide theory in the ‘spin basis’ has been described for the first time by us in this work (Ref.¹⁴).

Measuring the bond current density following the steps given in Appendix A, we determine current by integrating the current density using the relation

$$I_{n,n+1}(V) = \int_{-\infty}^{\infty} J_{n,n+1}(E) [f_S(E) - f_D(E)] dE \quad (5)$$

where

$$f_{S(D)} = \frac{1}{1 + e^{(E - \mu_{S(D)})/k_B \mathcal{T}}}$$

is the Fermi function for S(D), k_B is the Boltzmann constant and \mathcal{T} is the equilibrium temperature. μ_S and μ_D are the electro-chemical potentials and they are expressed as $\mu_S = E_F + eV/2$ and $\mu_D = E_F - eV/2$, respectively,

where V is the bias voltage and E_F is the equilibrium Fermi energy.

Using the individual bond currents, the net circular current is obtained through the sum^{10,14}

$$I_C = \frac{1}{N} \sum_n I_{n,n+1} \quad (6)$$

where N denotes the total number of lattice sites in the ring. In determining the current we assign a positive sign for the current propagating in the anti-clockwise direction.

The above expression i.e., Eq. 6 is one of the required quantities to analyze the logical operations, as mentioned. Now, the other key factor that needs to be evaluated is the induced magnetic field due to the circular current generated in the loop. The magnetic field at any arbitrary point (say) r is obtained using the well known Biot-Savart's law^{10,14}

$$\vec{B}(\vec{r}) = \sum_n \left(\frac{\mu_0}{4\pi} \right) \int I_{n,n+1} \frac{d\vec{r}' \times (\vec{r} - \vec{r}')}{|\vec{r} - \vec{r}'|^3} \quad (7)$$

where μ_0 is the magnetic constant.

In our analysis, the logical outputs (ON and OFF states) are described by the orientation of the local (free) spin placed at the ring center. The spin is initially aligned along a particular direction which we refer as 'OFF' state or low output, while in the presence of induced magnetic field when the free spin is aligned along $+Z$ direction we get the 'ON' state or high output. We calculate the angle of rotation θ_C because of the magnetic field B , assuming the operation time τ , from the condition^{31,32}

$$\theta_C = \frac{g\mu_B B \tau}{2\hbar} \quad (8)$$

where g is the Lande g -factor and μ_B is the Bohr magneton. Thus, if the relative angle θ_C is zero, the logical output becomes 'low', whereas the output is 'high' when the spin is aligned along Z direction.

Finally, to estimate the performance of logic circuits we compute power, delay and the product of these two. The power is easily determined, while the delay time is measured from the relation³³

$$\tau_d = \frac{(Q_{\text{on}} - Q_{\text{off}})}{I_{\text{on}}} \quad (9)$$

where Q_{on} and Q_{off} represent the charges in the ON and OFF states, respectively, and I_{on} corresponds to on-current.

The charge $Q_{\text{on(off)}}$ at the bias voltage V is obtained from the expression³⁴

$$Q_{\text{on(off)}} = C_{\text{on(off)}} V = |e|^2 \rho_{\text{on(off)}} V \quad (10)$$

where $C_{\text{on(off)}}$ is the quantum capacitance and $\rho_{\text{on(off)}}$ is the density of states.

III. NUMERICAL RESULTS AND DISCUSSION

The results are essentially arranged in two parts. One includes the individual logical operations, those are obtained by reconfiguring a single setup. The other part describes the parallel logic options. Both are very important and here we discuss them one by one. Before analyzing the results, let us mention the common parameter values those are taken into consideration throughout the numerical calculations. We consider a six-site ring as a basic building block. In the ring, the on-site energies $\epsilon_{n\uparrow} = \epsilon_{n\downarrow} = 0 \forall n$, and the NNH hopping strength $t = 0.5$ eV. These quantities (ϵ_0 and t_0) for the side attached electrodes are taken as 0 and 1 eV, respectively. The ring-to-electrode coupling strengths $t_S = t_D = 0.25$ eV. The spin flip parameter h_n for all the sites is also fixed at 0.25 eV. All the physical pictures of logic operations presented here remain unchanged for other choices of the parameter values as well, which we confirm through our rigorous numerical calculations. We take $\varphi_n = 0$ for all n . Unless stated otherwise, we compute all the results at absolute zero temperature and at $E_F = 0$.

As the central operations are associated with the orientation of the free spin placed at the ring center due to the induced magnetic field, first it is important to check

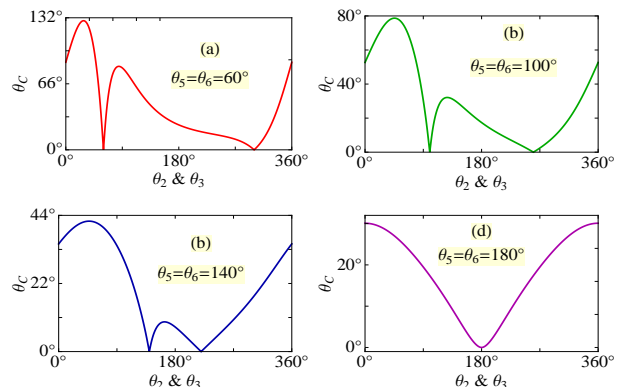


FIG. 2: (Color online). Angle of the rotation θ_C (measured in degree) of the free spin as a function of θ_2 ($= \theta_3$) for four different cases of θ_5 ($= \theta_6$). The bias voltage is set at $V = 0.25$ V.

the response of this free spin viz, the possible degree of rotation under different input conditions. More specifically, we want to examine whether the induced magnetic field is suitable enough to rotate the spin or not. The results are shown in Fig. 2 considering a similar kind of setup as taken in Fig. 1. We fix the alignments of spins at sites 5 and 6 (measured by θ_5 and θ_6), and rotate the spins at 2 and 3 (measured by θ_2 and θ_3) keeping them in parallel i.e., $\theta_2 = \theta_3$. Here we choose $\theta_1 = \theta_4 = 0$, and set the bias $V = 0.25$ V. A finite circular current, and thus magnetic field, is generated as long as the net current passing through one arm is different from the current flowing in the other arm, since the arm lengths are equal for our nano junction. Four different cases are shown, depending on the typical values of θ_5 ($= \theta_6$). In

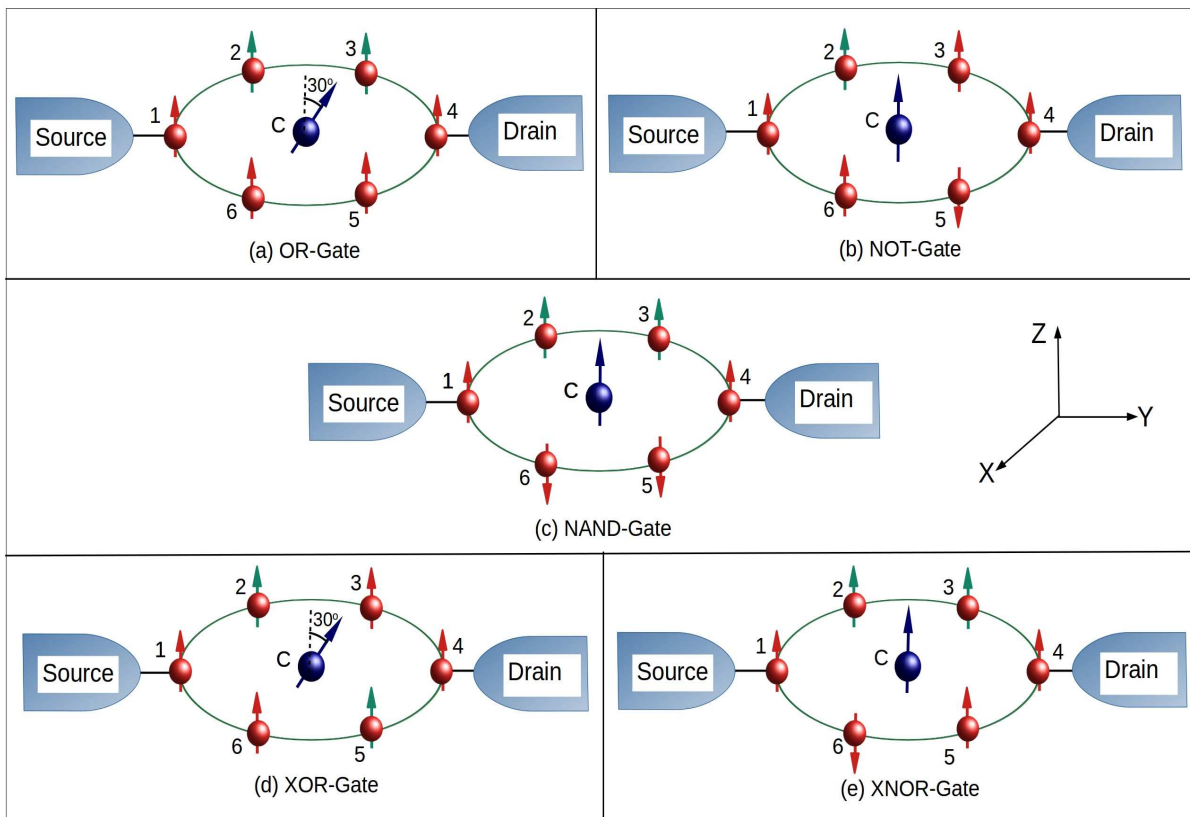


FIG. 3: (Color Online). Layouts of five different logical operations. The input conditions are imposed through the spins shown by the green color. When the spin is up it indicates 0 input state, while for the down spin the input state becomes 1. The free spin is initially orientated at 30° which describes the zero output condition. All these logical operations are in principle designed by reconfiguring a common basic structure.

each of these cases the angle of rotation θ_C of the free spin is determined, by measuring the magnetic field associated with I_C , following the relation given in Eq. 8. The orientations of the spins located at sites 2 and 3 are varied from 0 to 2π . Interestingly we see that the free spin can have a high degree of rotation (in one case it becomes more than 130°), depending on θ_5 ($=\theta_6$). This large degree of rotation is possible due to the generation of much higher magnetic field at the ring center. It clearly suggests that, the required magnetic field to rotate a free spin can easily be achieved, and this higher magnetic field is obtained mainly because of the smaller loop area of the ring. Thus, we can safely utilize this prescription to recognize two different states of the output. The vanishing rotation ($\theta_C = 0$) is observed only for the two typical situations. These are (i) θ_2 ($=\theta_3$) $=\theta_5$ ($=\theta_6$) and (ii) θ_2 ($=\theta_3$) $=2\pi - \theta_5$ ($=2\pi - \theta_6$). Under these conditions, the currents through the upper and lower arms of the ring become identical, resulting vanishing I_C and hence the induced magnetic field B .

A. Reprogrammable spin logic gate

With the above verification that a sufficient magnetic field can be generated at the ring center to rotate a free

spin, now we explain the logical operations. Figure 3 shows the setups of designing five logic gates, OR, NOT, NAND, XOR and XNOR, where all these logic gates are re-configured from a common basic structure. The spins shown by the green color are used to regulate the input states. When the spin is up we get 0 input state, while for down spin the input state becomes 1, and we follow this prescription throughout the discussion. The free spin, amended at the ring center, is aligned at an angle 30° with respect to the Z axis which represents the ‘low’ output state, and when it gets oriented along Z direction in presence of finite magnetic field at the ring center we get ‘high’ output state. Now, in order to rotate the spin by 30° , the minimum magnetic field that is required is ~ 2.4 mT (calculated by using Eq. 8). We measure the response i.e., the logical outputs in terms of the magnetic field under different input conditions. The results are described in a tabular form (see Table I) to have a clear picture of all the logical operations.

The selection of the input spin(s) is very crucial, as we need to satisfy the required ‘symmetric’ and ‘asymmetric’ conditions for getting zero and non-zero circular currents, and thus, induced magnetic field, to have all these kinds of logical operations. For instance, if we focus on the OR gate setup, we see that the spins at sites 2 and 3 are used to set the logical inputs, whereas for XOR gate

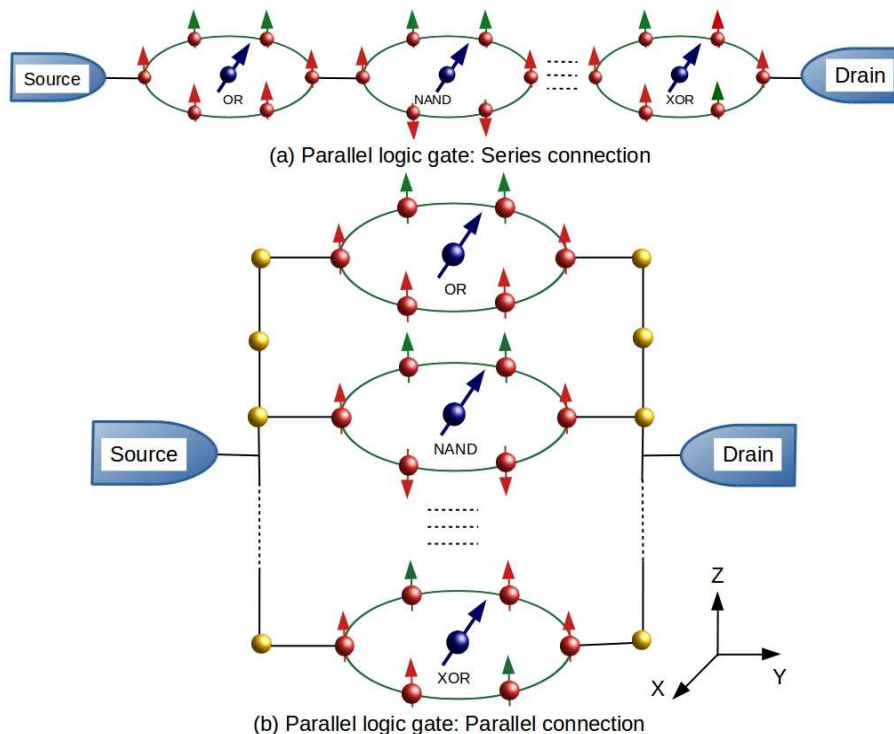


FIG. 4: (Color Online). Outline to achieve all possible logical operations in a single nanojunction device, where individual loops are used to serve different logic gates. All the colored spins correspond to the identical meaning as discussed in Fig. 3. The parallel operations are performed in ‘two ways’ by connecting the loops in (a) series and (b) parallel. In each of these diagrams, the dotted portion implies that we can add any number of rings representing different and/or identical logical operations in series or parallel.

TABLE I: Truth tables for different logical operations. Output is described in terms of the generated magnetic field (measured in unit of mT) at the loop center. The bias is fixed at $V = 0.25$ V.

Input		Output				NOT	
		OR	NAND	XOR	XNOR	Input	Output
↑	↑	0	2.5	0	40	↑	40
↑	↓	40	2.5	40	0	↓	0
↓	↑	40	2.5	40	0		
↓	↓	2.5	0	0	2.5		

the spins at sites 2 and 5 are considered. Not only that, we need to concentrate on the other spins as well (drawn by the red color) located at other sites, to satisfy the required conditions. But, the fact is that we develop all these logical operations by re-configuring a single setup. This is quite interesting and important as well which we strongly believe, and may give some impact in designing future nanoelectronic devices.

B. Parallel logic operations: Two prescriptions

The above sub-section (Sub-Sec. B) illustrates single logic operation at a particular time. As all the logic functions are based on the operation of the free spin due to

the induced magnetic field at the ring center, we can easily extrapolate this idea to implement several logic operations simultaneously, as many as we wish, in a single setup. Under this case, the performance of one logic gate is no longer disturbed by the others, which is the most important issue of our analysis. This feature is no longer expected from the earlier propositions of logic operations. Simultaneous operations can be obtained but they are highly limited, as in most of the cases one logic function can be influenced by the other. All these issues are successfully eliminated in our present proposal. Two separate schemes are explored to execute the parallel operations those are: (i) all logic gates are operated simultaneously in one setup and (ii) all possible inputs are given at a particular time and all the output signals are read simultaneously. These aspects are analyzed one by one as given below.

1. Designing of different logic gates in one setup

Here we emphasize on how to perform different logical operations at an identical time in a single junction device. It can be done in two ways, those are schematically illustrated in Figs. 4(a) and (b), where the loops, involving different logic gates, are connected in series and parallel, respectively. For individual logic gates, the architecture should be followed as discussed in Fig. 3 which

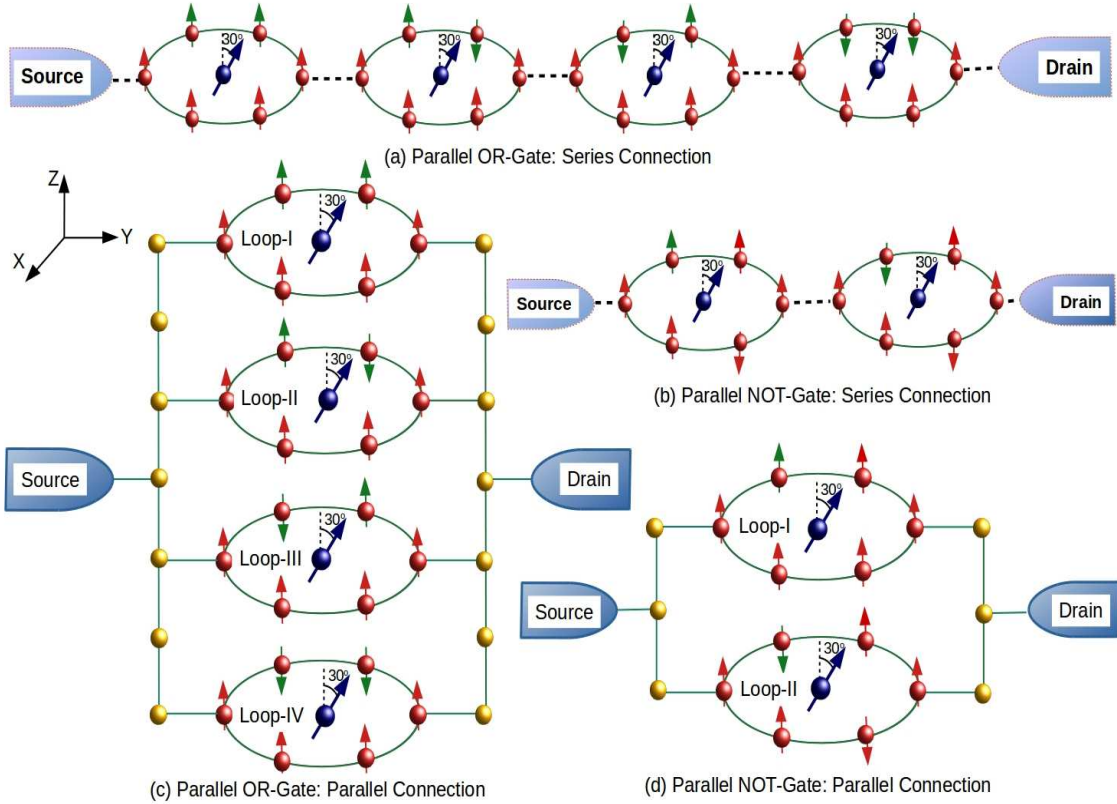


FIG. 5: (Color Online). Different mechanisms of getting parallel operations. All the inputs of a logic gate are implemented at one time, and all the outputs are read simultaneously. For a two-input logic gate total four loops, whereas for the two-input gate two loops are considered depending on the possible input conditions. We arrange them either in series or parallel, as schematically shown here. The different colored spins carry the usual meanings as mentioned earlier in other figures. Among all the two-input logic gates, here we show the operation of OR gate, as a typical example. Similar prescription is followed for the other two-input gates.

means we need to satisfy the identical ‘symmetric’ and ‘asymmetric’ conditions to get the operations. For the parallel connection of the ring conductors, it may seem that the circuit diagram is quite trivial and expected as well, since all these individual loops are getting identical power from the contact electrodes, like what we have for different functional elements in conventional CPUs in PCs. But, for better clarity and clear understanding we expose both the two possibilities (series and parallel) for simultaneous logic operations. Unlike parallel connection, the loops are not getting identical power when they are coupled in series, although we can fully satisfy our purpose. Thus, designing of all possible logic gates at a same time is of course possible.

2. Parallel operations in a single logic gate

Designing of a logic gate where all the inputs are given in parallel and all the outputs are also read simultaneously is undoubtedly extremely significant. So far only one work is available¹⁶ along this line, though the functional operations described in that work are not spin based. Now, to satisfy the parallelized conditions in our spin based device, we have to couple four or two loops

depending on whether it is two-input or one-input logic gate, as for a two-input gate there are four possible input (output) conditions, while for the other case two input

TABLE II: Truth tables for different parallel logical operations where the loops are connected in series configuration. Output response is described in terms of the induced magnetic field (measured in unit of mT) at the loop centers.

	Input	Output				NOT	
		OR	NAND	XOR	XNOR	Input	Output
Loop-1	↑ ↑	0	49	0	94	↑	4.7
Loop-2	↑ ↓	4.4	14	10	0	↓	0
Loop-3	↓ ↑	4.4	14	10	0		
Loop-4	↓ ↓	4.9	0	0	8.4		

(output) conditions are there. Among all the possible two-input gates, here we take OR gate as a prototype example to explain the parallel operation, and all the other such gates can be described in the same footing. Together with OR gate, we also consider NOT gate to discuss the operation for the one-input logic gate.

The schematic arrangements of the loops for designing the parallel OR and NOT gates are shown in Fig. 5. Both the series and parallel configurations of the loops

TABLE III: Same as Table II, when the loops are arranged in parallel configuration.

	Input		Output				NOT	
			OR	NAND	XOR	XNOR	Input	Output
Loop-1	↑	↑	0	8.9	0	5	↑	16.2
Loop-2	↑	↓	18.5	9.4	13.8	0	↓	0
Loop-3	↓	↑	14	5.8	20	0		
Loop-4	↓	↓	3.6	0	0	6.8		

are taken into account, where each loop is associated with one logical input condition, and the output is measured by the response of the free spin embedded at the ring center, like previous operations. Both for the series and parallel configurations, the response of any loop gets no longer disturbed by the responses of the other loops. They work well independently, which is the notable feature of our prescription. These logical functions cannot be performed if the operations are made using the concept of the conventional transport current, since the vanishing transport current across any loop stops the current flow through all other loops, which essentially gives

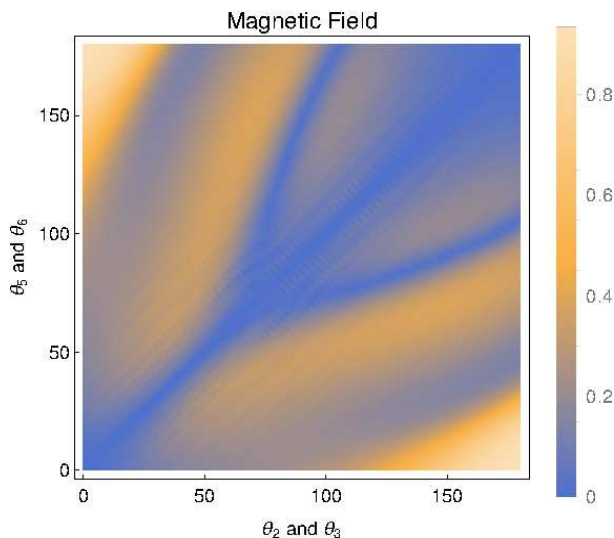


FIG. 6: (Color Online). Density plot of induced magnetic field at the ring center, associated with the circular current, as functions of $\theta_2 (= \theta_3)$ and $\theta_5 (= \theta_6)$. Here we take the nanojunction as shown in Fig. 1, and compute the results at the bias voltage $V = 2$ V. The system temperature is fixed at $\mathcal{T} = 300$ K.

a null state (i.e., the circuit becomes off). On the other hand, the vanishing circular current in any loop under the symmetric condition does not yield vanishing transport current, and therefore, we can safely perform the required operations.

The responses of different logic gates are shown in tabular form. In Table II, the results are presented when the loops are configured in series. To have better output, we fix the bias voltage $V = 0.25$ V for the OR, XOR and NOT gates, while for the other two gates (NAND and XNOR) we set $V = 0.7$ V. These biases are not specific, and any other voltage can also be taken into account.

For the case of parallel configuration of the rings, the results are given in Table III. Here we choose the biases as $V = 0.6$ V and 0.7 V like the above sets of logic gates. Both from Table II and Table III, the logical responses are clearly reflected, and thus we can emphasize that the parallel operations can be substantiated where all the inputs are switched on together and outputs are read at an identical time.

C. Effect of temperature

All the results presented above are worked out at zero temperature. Keeping in mind the realistic situation, now we want to examine whether the above facts are still valid even at moderate temperature or not. This checking is always crucial for device designing. The another fact is that, in the above analysis we consider up and down spin orientations as the two input states, and thus we align other spins to get the required symmetric and asymmetric conditions to establish the logical operations. Instead of these, one can also consider any other arrangements of the input states and accordingly we need to align the other spins to reach the required conditions. In any such arrangements we have to make sure that the induced magnetic field is sufficient enough to rotate the free spin in desired angle to achieve the high output state.

In Fig. 6, we show a density plot of the induced magnetic field at the ring center, considering a similar kind of nanojunction as taken in Fig. 1, by simultaneously varying $\theta_2 (= \theta_3)$ and $\theta_5 (= \theta_6)$. The results are computed at the bias voltage $V = 2$ V, setting the temperature $\mathcal{T} = 300$ K. Clearly we see that, for a wide range of θ_2 and θ_5 considerably large magnetic field is induced because of the non-zero circular current in the ring. At finite temperature, since all the energy levels contribute to the current, there is a possibility to get smaller spin dependent circular current due to mutual cancellations, and hence the magnetic field. But for our case we still get a reasonably large circular current to satisfy the required logic operations. Thus, all the logical operations stated here can be achieved in realistic situation and we believe that the proposal can be verified in suitable laboratories.

D. Power, delay and power-delay-product

Consumption of lower power and much faster operation i.e., lesser delay time are the two important prerequisites to get an efficient device. The efficiency can be quantified in a more general way by calculating the product of the power and the delay time. The PDP is called as the *figure of merit* which measures the energy consumed in each operation. What we find from our extensive calculations is that the PDP is extremely small for all the logical operations studied in this work. In Table IV we present the results of some of them, and they are single OR gate, parallel OR gate for the series connection (which we refer in the table as parallel OR gate I), and parallel OR gate for the parallel connection

TABLE IV: Power, delay, and PDP of various logic devices at $V = 0.25$ V and $E_F = 0.75$ eV.

	Delay (s)	Power (W)	PDP (J)
OR Gate	7.78×10^{-16}	1.55×10^{-8}	1.21×10^{-23}
Parallel OR Gate I	2.24×10^{-12}	9.07×10^{-14}	2.03×10^{-25}
Parallel OR Gate II	3.86×10^{-15}	5.28×10^{-11}	2.04×10^{-25}

(which is mentioned in the table as parallel OR gate II). For other logic gates the delay, power and PDP are of the same orders of magnitude as given in Table IV. All the quantities are very low compared to the traditional TTL and CMOS logic families. The underlying mechanism relies on the fact that all the operations discussed here are performed based on the ‘spin states’ unlike the conventional logic functions where charges are taken into account for the logic inputs and/or outputs. The factors shown in Table IV remain almost unchanged even for much higher bias voltages which we confirm through our numerous numerical calculations. With these results we can strongly argue that the proposed logic operations are superior than the existing logic families.

E. Experimental realization of magnetic nano rings

Finally, we discuss how to realize magnetic nano rings experimentally those are used to have logical operations. Several prescriptions are available in literature and with the help of those advanced methodologies it is now possible to get simple and complex patterned magnetic ring geometries. For instance here we want to highlight some of those approaches for the benefit of readers. The most common techniques to design magnetic rings are the electron beam lithography³⁵, silicon etching processes³⁶ and the nanosphere lithography^{37,38}. Sometimes droplet epitaxy method³⁹ is also used for the fabrication of ring like geometries. Using this prescription, Mano *et al.*⁴⁰ have designed magnetic rings with diameters of the order of few nm, and also suggested how to tune the size of the magnetic rings. Yang and co-workers have claimed in their work that more controlled magnetic rings can be constructed by dewetting magnetic nanoparticle solution in a specific substrate⁴¹. With these enormous possibilities, we hope that magnetic nano rings of desired radius can be fabricated, and the orientations of selective spins at distinct magnetic sites can be controlled selectively following the prescriptions discussed earlier. Thus our propositions of logic operations using magnetic rings can be tested in a suitable laboratory setup.

IV. CLOSING REMARKS

The work essentially deals with the possible designing mechanisms of logic gates at nano-scale level, where everything is ‘spin based’, circumventing the traditional prescription of getting ‘charge based’ ones. Few contemporary proposals are already available, though such a

comprehensive analysis, presented here, using the concept of ‘bias driven spin based circular current in a nano loop’ does not exist in literature to the best of our concern. Their key aspects and finding of our work are summarized as follows.

- Before presenting the results, we have checked whether the circular current induced magnetic field is sufficient enough to rotate a free spin in desired angle. What we have found is that, a high degree of rotation can be made as the induced magnetic field is considerably large. This high magnetic field is achieved mainly due to the small size ring.
- Following this verification, we have discussed how to substantiate logical operations. Total five logic gates have been designed.
- In the rest part of our analysis we have mostly focussed on the principle of getting parallel logic operations. Here two different prescriptions have been proposed. In one case all the logic gates can be operated simultaneously, while in the other prescription a single logic gate has been taken into account where all the inputs can be implemented at a same time and also all the outputs can be read simultaneously. Both these two proposals are interesting and important as well.
- In the construction of parallel operations, the most notable point is that one logical operation gets no longer disturbed by the other. Since the operations depend entirely on the generated circular current, not on the transport current, we can get simultaneous operations from individual nano rings, whether they are connected in series or parallel.
- We have also discussed the effects of temperature, and found that all the logical operations are equally valid even at moderate temperatures.
- We have tested the efficiency of the logic circuits by studying power, delay and PDP. From our results we have reached to the conclusion that all the logic functions studied here are quite superior than the conventional logic families.
- Finally, we have given a brief outline about the designing principle of nano rings, for the sake of completeness of our analysis.

We end by stating that, the present analysis can give a boost in the field of reconfigurable logic operations since all the logic gates are designed by rearranging the spins in a single setup. The device in one hand is very simple to understand and on the other hand it can probably be designed quite easily in advanced laboratories.

ACKNOWLEDGMENT

SKM would like to thank the financial support of DST-SERB, Government of India, through the Project Grant Number EMR/2017/000504.

Appendix A: Calculation of current density from the set of coupled equations

Both for incident up and down spin electrons, we need to write a separate set of coupled equations. Let us be-

gin with an up spin electron which gets injected from the source end to the ring system as a plane wave with unit amplitude. For the nanojunction shown Fig. 1, the set of coupled equations are expressed, in general forms (considering $\epsilon_{n\uparrow} = \epsilon_{n\downarrow} = \epsilon_n$) as follows:

$$\begin{aligned}
& \left[\begin{pmatrix} E & 0 \\ 0 & E \end{pmatrix} - \begin{pmatrix} \epsilon_0 & 0 \\ 0 & \epsilon_0 \end{pmatrix} \right] \begin{pmatrix} 1 + \rho_{\uparrow\uparrow} \\ \rho_{\uparrow\downarrow} \end{pmatrix} = \begin{pmatrix} t_0 & 0 \\ 0 & t_0 \end{pmatrix} \begin{pmatrix} e^{-ika} + \rho_{\uparrow\uparrow} e^{ika} \\ \rho_{\uparrow\downarrow} e^{ika} \end{pmatrix} + \begin{pmatrix} t_S & 0 \\ 0 & t_S \end{pmatrix} \begin{pmatrix} C_{1,\uparrow} & 0 \\ 0 & C_{1,\downarrow} \end{pmatrix} \\
& \left[\begin{pmatrix} E & 0 \\ 0 & E \end{pmatrix} - \begin{pmatrix} \epsilon_1 + h_1 \cos \theta_1 & \sin \theta_1 e^{-i\varphi_1} \\ \sin \theta_1 e^{i\varphi_1} & \epsilon_1 - h_1 \cos \theta_1 \end{pmatrix} \right] \begin{pmatrix} C_{1,\uparrow} & 0 \\ 0 & C_{1,\downarrow} \end{pmatrix} = \begin{pmatrix} t_S & 0 \\ 0 & t_S \end{pmatrix} \begin{pmatrix} 1 + \rho_{\uparrow\uparrow(S)} \\ \rho_{\uparrow\downarrow(S)} \end{pmatrix} + \begin{pmatrix} t & 0 \\ 0 & t \end{pmatrix} \begin{pmatrix} C_{2,\uparrow} & 0 \\ 0 & C_{2,\downarrow} \end{pmatrix} \\
& \hspace{15em} + \begin{pmatrix} t & 0 \\ 0 & t \end{pmatrix} \begin{pmatrix} C_{6,\uparrow} & 0 \\ 0 & C_{6,\downarrow} \end{pmatrix} \\
& \left[\begin{pmatrix} E & 0 \\ 0 & E \end{pmatrix} - \begin{pmatrix} \epsilon_2 + h_2 \cos \theta_2 & \sin \theta_2 e^{-i\varphi_2} \\ \sin \theta_2 e^{i\varphi_2} & \epsilon_2 - h_2 \cos \theta_2 \end{pmatrix} \right] \begin{pmatrix} C_{2,\uparrow} & 0 \\ 0 & C_{2,\downarrow} \end{pmatrix} = \begin{pmatrix} t & 0 \\ 0 & t \end{pmatrix} \begin{pmatrix} C_{1,\uparrow} & 0 \\ 0 & C_{1,\downarrow} \end{pmatrix} + \begin{pmatrix} t & 0 \\ 0 & t \end{pmatrix} \begin{pmatrix} C_{3,\uparrow} & 0 \\ 0 & C_{3,\downarrow} \end{pmatrix} \\
& \left[\begin{pmatrix} E & 0 \\ 0 & E \end{pmatrix} - \begin{pmatrix} \epsilon_3 + h_3 \cos \theta_3 & \sin \theta_3 e^{-i\varphi_3} \\ \sin \theta_3 e^{i\varphi_3} & \epsilon_3 - h_3 \cos \theta_3 \end{pmatrix} \right] \begin{pmatrix} C_{3,\uparrow} & 0 \\ 0 & C_{3,\downarrow} \end{pmatrix} = \begin{pmatrix} t & 0 \\ 0 & t \end{pmatrix} \begin{pmatrix} C_{2,\uparrow} & 0 \\ 0 & C_{2,\downarrow} \end{pmatrix} + \begin{pmatrix} t & 0 \\ 0 & t \end{pmatrix} \begin{pmatrix} C_{4,\uparrow} & 0 \\ 0 & C_{4,\downarrow} \end{pmatrix} \\
& \left[\begin{pmatrix} E & 0 \\ 0 & E \end{pmatrix} - \begin{pmatrix} \epsilon_4 + h_4 \cos \theta_4 & \sin \theta_4 e^{-i\varphi_4} \\ \sin \theta_4 e^{i\varphi_4} & \epsilon_4 - h_4 \cos \theta_4 \end{pmatrix} \right] \begin{pmatrix} C_{4,\uparrow} & 0 \\ 0 & C_{4,\downarrow} \end{pmatrix} = \begin{pmatrix} t & 0 \\ 0 & t \end{pmatrix} \begin{pmatrix} C_{3,\uparrow} & 0 \\ 0 & C_{3,\downarrow} \end{pmatrix} + \begin{pmatrix} t & 0 \\ 0 & t \end{pmatrix} \begin{pmatrix} C_{5,\uparrow} & 0 \\ 0 & C_{5,\downarrow} \end{pmatrix} \\
& \hspace{15em} + \begin{pmatrix} t_D & 0 \\ 0 & t_D \end{pmatrix} \begin{pmatrix} \tau_{\uparrow\uparrow} e^{ika} \\ \tau_{\uparrow\downarrow} e^{ika} \end{pmatrix} \\
& \left[\begin{pmatrix} E & 0 \\ 0 & E \end{pmatrix} - \begin{pmatrix} \epsilon_5 + h_5 \cos \theta_5 & \sin \theta_5 e^{-i\varphi_5} \\ \sin \theta_5 e^{i\varphi_5} & \epsilon_5 - h_5 \cos \theta_5 \end{pmatrix} \right] \begin{pmatrix} C_{5,\uparrow} & 0 \\ 0 & C_{5,\downarrow} \end{pmatrix} = \begin{pmatrix} t & 0 \\ 0 & t \end{pmatrix} \begin{pmatrix} C_{4,\uparrow} & 0 \\ 0 & C_{4,\downarrow} \end{pmatrix} + \begin{pmatrix} t & 0 \\ 0 & t \end{pmatrix} \begin{pmatrix} C_{6,\uparrow} & 0 \\ 0 & C_{6,\downarrow} \end{pmatrix} \\
& \left[\begin{pmatrix} E & 0 \\ 0 & E \end{pmatrix} - \begin{pmatrix} \epsilon_6 + h_6 \cos \theta_6 & \sin \theta_6 e^{-i\varphi_6} \\ \sin \theta_6 e^{i\varphi_6} & \epsilon_6 - h_6 \cos \theta_6 \end{pmatrix} \right] \begin{pmatrix} C_{6,\uparrow} & 0 \\ 0 & C_{6,\downarrow} \end{pmatrix} = \begin{pmatrix} t & 0 \\ 0 & t \end{pmatrix} \begin{pmatrix} C_{5,\uparrow} & 0 \\ 0 & C_{5,\downarrow} \end{pmatrix} + \begin{pmatrix} t & 0 \\ 0 & t \end{pmatrix} \begin{pmatrix} C_{1,\uparrow} & 0 \\ 0 & C_{1,\downarrow} \end{pmatrix} \\
& \left[\begin{pmatrix} E & 0 \\ 0 & E \end{pmatrix} - \begin{pmatrix} \epsilon_0 & 0 \\ 0 & \epsilon_0 \end{pmatrix} \right] \begin{pmatrix} 1 + \tau_{\uparrow\uparrow} \\ \tau_{\uparrow\downarrow} \end{pmatrix} = \begin{pmatrix} t & 0 \\ 0 & t \end{pmatrix} \begin{pmatrix} C_{4,\uparrow} & 0 \\ 0 & C_{4,\downarrow} \end{pmatrix} + \begin{pmatrix} t_0 & 0 \\ 0 & t_0 \end{pmatrix} \begin{pmatrix} \tau_{\uparrow\uparrow} e^{2ika} \\ \tau_{\uparrow\downarrow} e^{2ika} \end{pmatrix}
\end{aligned} \tag{A1}$$

The factors $\rho_{\sigma\sigma'}$ and $\tau_{\sigma\sigma'}$ correspond to the spin dependent reflection and transmission amplitudes, respectively, k is the wave vector and a is the inter-atomic distance.

Solving Eq. A1, we get all the required co-efficients, and, then the bond current density between any bond connecting the sites n and $(n+1)$ is obtained from the relation

$$J_{n,n+1,\sigma\sigma'}(E) = \frac{(2e/\hbar)\text{Im} [t C_{n,\sigma\sigma'}^* C_{i+1,\sigma\sigma'}]}{(2e/\hbar)(1/2)t_0 \sin(ka)}. \tag{A2}$$

Here σ is used for the incident spin, while σ' denotes the transmitting spin.

In the same footing we can write another set of coupled equations for the down spin electron, and determining the co-efficients we compute $J_{n \rightarrow n+1\downarrow}$ and $J_{n \rightarrow n+1\uparrow}$.

Once we have all these components involving circular bond current densities, we finally obtain the net bond current density $J_{n,n+1}$ by the relation

$$J_{n,n+1}(E) = J_{n,n+1,\uparrow\uparrow} + J_{n,n+1,\uparrow\downarrow} + J_{n,n+1,\downarrow\downarrow} + J_{n,n+1,\downarrow\uparrow}. \tag{A3}$$

The above prescription can now easily be generalized for any junction setup.

* Electronic address: moumita.patra19@gmail.com

† Electronic address: shukla@phy.iitb.ac.in

‡ Electronic address: santanu.maiti@isical.ac.in

¹ A. Ney, C. Pampuch, R. Koch, and K. H. Ploog, *Nature* **425**, 485 (2003).

² S. A. Wolf *et al.*, *Science* **294**, 1488 (2001).

³ D. E. Nikonov, G. I. Bourianoff, and P. A. Gargini, *J. Supercond. Novel Magn.* **19**, 497 (2006).

⁴ M. Johnson and R. H. Silsbee, *Phys. Rev. Lett.* **55**, 1790 (1985).

⁵ M. N. Baibich *et al.*, *Phys. Rev. Lett.* **61**, 2472 (1988).

⁶ A. Nakanishi and M. Tsukada, *Phys. Rev. Lett.* **87**, 126801 (2001).

⁷ K. Tagami and M. Tsukada, *Curr. Appl. Phys.* **3**, 439 (2003).

⁸ M. Tsukada, K. Tagami, K. Hirose, and N. Kobayashi, *J.*

- Phys. Soc. Jpn. **74**, 1079 (2005).
- ⁹ G. Stefanucci, E. Perfetto, S. Bellucci, and M. Cini, Phys. Rev. B **79**, 073406 (2009).
 - ¹⁰ D. Rai, O. Hod, and A. Nitzan, J. Phys. Chem. C **114**, 20583 (2010).
 - ¹¹ D. Rai, O. Hod, and A. Nitzan, Phys. Rev. B **85**, 155440 (2012).
 - ¹² M. Patra and S. K. Maiti, Org. Electron. **62**, 454 (2018).
 - ¹³ M. Patra and S. K. Maiti, Sci. Rep. **7**, 43343 (2017).
 - ¹⁴ M. Patra and S. K. Maiti, Phys. Rev. B **100**, 165408 (2019).
 - ¹⁵ B. Behin-Aein, D. Datta, S. Salahuddin, and S. Datta, Nature Nanotech. **5**, 266 (2010).
 - ¹⁶ B. Fresch, M. Cipolloni, T.-M. Yan, E. Collini, R. D. Levine, and F. Remacle, J. Phys. Chem. Lett. **6**, 1714 (2015).
 - ¹⁷ Y. Xu, X. Jin, and H. Zhang, Phys. Rev. E **88**, 052721 (2013).
 - ¹⁸ A. Dari, B. Kia, A. R. Bulsara, and W. L. Ditto, Europhys. Lett. **93**, 18001 (2011).
 - ¹⁹ H. Ando, S. Sinha, R. Storni, and K. Aihara K., Europhys. Lett. **93**, 50001 (2011).
 - ²⁰ M. Patra and S. K. Maiti, Europhys. Lett. **123**, 58008 (2018).
 - ²¹ M. Patra and S. K. Maiti, Europhys. Lett. **121**, 38004 (2018).
 - ²² F. H. L. Koppens, K. C. Nowack, and L. M. K. Vandersypen, Phys. Rev. Lett. **100**, 236802 (2008).
 - ²³ Y. Tokura, W. G. van der Wiel, T. Obata, and S. Tarucha, Phys. Rev. Lett. **96**, 047202 (2006).
 - ²⁴ K. C. Nowack, F. H. L. Koppens, Y. V. Nazarov, and L. M. K. Vandersypen, Science **318**, 1430 (2007).
 - ²⁵ K.-M. C. Fu, S. M. Clark, C. Santori, C. R. Stanley, M. C. Holland, and Y. Yamamoto, Nat. Phys. **4**, 780 (2008).
 - ²⁶ J. Berezovsky, M. H. Mikkelsen, N. G. Stoltz, L. A. Col-dren, and D. D. Awschalom, Science **320**, 349 (2008).
 - ²⁷ Y. Wu, E. D. Kim, X. Xu, J. Cheng, D. G. Steel, A. S. Bracker, D. Gammon, S. E. Economou, and L. J. Sham, Phys. Rev. Lett. **99**, 097402 (2007).
 - ²⁸ D. Press, T. D. Ladd, B. Zhang, and Y. Yamamoto, Nature **456**, 218 (2008).
 - ²⁹ Y. -H. Su, S. -H. Chen, C. D. Hu, and C.-R. Chang, J. Phys.D: Appl. Phys. **49**, 015305 (2016).
 - ³⁰ S. Sarkar and S. K. Maiti, Phys. Rev. B **100**, 205402 (2019).
 - ³¹ D. A. Lidar and J. H. Thywissen, J. Appl. Phys. **96**, 754 (2004).
 - ³² S. K. Maiti, J. Appl. Phys. **117**, 024306 (2015).
 - ³³ W. Wang, Y. Sun, H. Wang, H. Xu, M. Xu, S. Jiang, and G. Yue, Semicond. Sci. Technol. **31**, 035002 (2016).
 - ³⁴ S. Dröscher, P. Roulleau, F. Molitor, P. Studerus, C. Stampfer, K. Ensslin, and T. Ihn, Appl. Phys. Lett. **96**, 152104 (2010).
 - ³⁵ E. M. Q. Jariwala, P. Mohanty, M. B. Ketchen, and R. A. Webb, Phys. Rev. Lett. **86**, 1594 (2001).
 - ³⁶ Z. Cui, J. Rothman, M. Klaui, L. Lopez-Diaz, and C. A. F. Vaz, and J. A. C. Bland, Microelectron. Eng. **61–62**, 577 (2002).
 - ³⁷ M. Winzer, M. Kleiber, N. Dix, and R. Wiesendanger, Appl. Phys. A **63**, 617 (1996).
 - ³⁸ S. M. Weekes, F. Y. Ogrin, and W. A. Murray, Langmuir **20**, 11208 (2004).
 - ³⁹ C. Z. Tong and S. F. Yoon, Nanotechnology **19**, 365604 (2008).
 - ⁴⁰ T. Mano, T. Kuroda, S. Sanguinetti, T. Ochiai, T. Tateno, J. Kim, T. Noda, M. Kawabe, K. Sakoda, G. Kido, and N. Koguchi, Nano Lett. **5**, 425 (2005).
 - ⁴¹ L. An, W. Li, Y. Nie, B. Xie, Z. Li, J. Zhang, and B. Yang, J. Colloid Interface Sci. **288**, 503 (2005).